Peptoid-based PET imaging of vascular endothelial growth factor receptor (VEGFR) expression

Guiyang Hao[1]; Asghar Hajibeigi[1]; Luis M. De León-Rodríguez[2]; Orhan K. Öz[1*]; Xiankai Sun[1,3]

[1]Department of Radiology, [3]Advanced Imaging Research Center, The University of Texas Southwestern Medical Center at Dallas, Dallas, TX, USA;. [2]Departmento de Química, Universidad de Guanajuato, Guanajuato, Mexico.

E-mails for all authors:

Guiyang Hao: guiyang.hao@utsouthwestern.edu

Asghar Hajibeigi: asghar.hajibeigi@utsouthwestern.edu

Luis M. De León-Rodríguez: lmdeleon@quijote.ugto.mx

Orhan K. Öz: orhan.oz@utsouthwestern.edu

Xiankai Sun: xiankai.sun@utsouthwestern.edu

Running title: Peptoid-based PET probe development

Corresponding author: Dr. Xiankai Sun, Department of Radiology, Advanced Imaging Research Center, The University of Texas Southwestern Medical Center at Dallas, Dallas, TX, USA. E-mail: xiankai.sun@utsouthwestern.edu

Abstract: Non-invasive detection of vascular endothelial growth factor receptor 2 (VEGFR2) by positron emission tomography (PET) would allow the evaluation of tumor vascular activity *in vivo*. Recently, a dimeric peptoid, GU40C4, was reported as a highly potent antagonist of VEGFR2 activation inhibiting angiogenesis and tumor growth *in vivo*. The purpose of this work was to evaluate the potential of this peptoid for PET imaging of VEGFR2 expression. To label GU40C4 and a control peptoid with a positron emitter, ^{64}Cu ($t_{1/2}$ = 12.7 h; β^+: 0.653 MeV, 17.4%), a cysteine was introduced to the C-terminus of the peptoids and then conjugated to a bifunctional chelator (DOTA: 1,4,7,10-tetraazacyclododecane-1,4,7,10-tetraacetic acid) through the maleimide-thiol coupling chemistry. The *in vitro* binding assay showed a negligible effect of the DOTA conjugation on the VEGFR2 binding affinity of GU40C4. Both peptoid conjugates were efficiently labeled with ^{64}Cu in high radiochemical yields (> 90%); the specific activity was in the range of 10 – 80 GBq/μmol. PET imaging evaluation using a prostate cancer xenograft (PC3) mouse model showed that ^{64}Cu-DOTA-GU40C4 had a prominent and steady accumulation in the VEGFR2 positive PC3 tumors (2.25 ± 0.24, 2.15 ± 0.34, and 1.90 ± 0.18 %ID/g at 1, 4, and 20 h p.i., respectively; n = 3), which is significantly higher than the control peptoid conjugate (0.3 – 0.5 %ID/g; $p < 0.001$ at 1, 4, and 20 h p.i.). Interestingly, the mouse salivary glands were also clearly visualized by ^{64}Cu-DOTA-GU40C4 (3.17 ± 0.25, 3.00 ± 0.36, and 1.83 ± 0.21 %ID/g at 1, 4, and 20 h p.i., respectively; n = 3) rather than its control peptoid conjugate. VEGFR2 expression in the salivary glands was shown by polymerase chain reaction (PCR) assay. Our results demonstrate that ^{64}Cu-DOTA-GU40C4 can be used to image the expression of VEGFR2 *in vivo*.

Keywords: VEGFR2, peptoid, PET, ^{64}Cu, prostate cancer, tumor angiogenesis

Introduction

Angiogenesis plays a crucial role in tumor progression and metastasis, especially when solid tumors grow beyond the size of 2 – 3 mm^3 [1, 2]. Represented by the US FDA approved bevacizumab (Avastin®), antiangiogenic therapy has been proven to be effective in cancer treatment. It would be desirable to have a non-invasive imaging technique for longitudinally monitoring the status of tumor angiogenesis for cancer prognosis. Given their inherent high sensitivity and capability of imaging quantitation, positron emission tomography (PET) and single photon emission computed tomography (SPECT) have become standard imaging techniques in clinical practice and molecular imaging research. To date, several biomarkers of angiogenesis have been identified and exploited as imaging targets. Among them, vascular endothelial growth factor receptor 2 (VEGFR2) and the $\alpha_v\beta_3$ integrin have drawn considerable attention [2]. VEGFR2 mediates the effects of the endothelial-specific mitogen VEGF on cell proliferation and permeability [3]. Upregulated expression of VEGFR2 has been reported in many tumor types (e.g. lung, colon, uterus, ovarian, prostate and breast cancer) with variable levels [3]. Indeed, several SPECT (^{123}I-VEGF$_{165}$ [4], ^{99m}Tc-VEGF$_{121}$ [5], ^{111}In-hnTf-VEGF [6]) and PET (^{64}Cu-DOTA-VEGF$_{121}$ [7], ^{64}Cu-DOTA-VEGF$_{DEE}$ [8]) imaging agents have been reported for imaging VEGFR2 expression. However, all the reported studies were done with natural/mutated VEGF-based isoforms. Although the imaging results are encouraging, the inherent limitations are obvious. For instance, these isoforms are generally difficult and costly to prepare in large scale; and the *in vivo* kinetics is not optimal for imaging because of their large size. In addition, they may induce an immune reaction *in vivo*.

Peptoids, oligomers of *N*-substituted glycines, are a specific subclass of peptidomimetics developed for drug discovery in the early 1990's [9]. They are closely related to their natural peptide counterparts, but the side chains of peptoids are appended to nitrogen atoms along the molecule's backbone rather than the α-carbon as in peptides. Due to the chemical difference, peptoids are peptidase/proteinase resistant. Peptoids are easier and more cost efficient to synthesize than peptides and can be used to generate large chemically diverse libraries for drug screening purposes. It has been demonstrated that libraries of peptoids are rich sources of protein-binding ligands [10] and are non-immunogenic in mice [11]. Recently, a VEGFR2 binding peptoid sequence (GU40C, monomer) was selected by a large library screening [10]. In light of the homo-dimer formation of VEGF receptors, the homo-dimer of GU40C, GU40C4, was therefore developed and validated with high potency against the VEGFR2 activation (K_d = 30 nM) [10]. To date, these peptoids and derivatives have been used to develop new cancer therapeutic and imaging agents. For instance, GU40C4 was conjugated at the C-terminal ends with two units of Ru(II)(tris-bipyridyl)$^{2+}$, which is an efficient photosensitizer of singlet oxygen production. The resulting conjugate proved to exhibit highly specific and potent VEGFR2 inactivation upon irradiation with visible light when compared to the peptoid itself [12]. In a recent report, GU40C4 was coupled to a lysine based dendron which contained eight individual Gd^{3+}-DOTA units for *in vivo* detection of VEGFR2 *via* Magnetic Resonance Imaging (MRI) [13]. Given its relative small size, high *in vivo* stability, and high binding affinity to VEGFR2, we set out to test the application of GU40C4 in specific PET imaging of VEGFR2. In this

study, we report the evaluation of this dimeric peptoid when labeled with ^{64}Cu ($t_{1/2}$ = 12.7 h; β^+: 0.653 MeV, 17.4%) in a prostate cancer mouse model.

Materials and methods

All chemicals were of reagent grade and used as received. All chemicals, solvents, and reagents were purchased from Sigma-Aldrich unless otherwise noted. Instant thin-layer chromatography (ITLC-SG) plates were purchased from Pall Life Sciences (East Hills, NY). Copper-64 chloride in 0.1 N HCl was purchased from University of Wisconsin at Madison. Light C-18 Sep-Pak cartridges were purchased from Waters (Milford, MA). Milli-Q water (18 MΩ-cm) was obtained from a Millipore Gradient Milli-Q water system (Billerica, MA). All aqueous solutions were prepared in deoxygenated Milli-Q water. High-performance liquid chromatography (HPLC) was performed on a Waters 600 Multisolvent Delivery System using a Waters Xterra column (250 × 10 mm, 10 μm). The HPLC system was equipped with a Waters 2996 Photodiode Array (PDA) detector and an in-line Shell Jr. 2000 radio-detector (Fredericksburg, VA). The mobile phases were H_2O with 0.1% TFA (solvent A) and acetonitrile with 0.1% TFA (solvent B). The gradient (I) consisted of 10 %B to 70 %B in 30 min at 4.0 mL/min; the gradient (II) consisted of 0 %B to 80 %B in 40 min at 4.0 mL/min. The matrix-assisted laser desorption/ionization – time-of-flight mass spectra (MALDI-TOF/MS) were recorded with a Voyager-DE™ PRO mass spectrometer with a Biospectrometry Workstation (Applied Biosystems). Radio-TLC analysis was performed on a Rita Star Radioisotope TLC Analyzer (Straubenhardt, Germany).

Cell culture and animal model

The PC3 cell line was obtained from the American Type Culture Collection (ATCC, Manassas, VA). PC3 cells were cultured in T-media (Invitrogen Corporation, Carlsbad, CA) supplemented with 5% FBS and 1×Penicillin/Streptomycin. The cells were cultured at 37 °C in an atmosphere of 5% CO_2 and passaged at 75 % confluence. Male SCID mice (6 – 8 weeks of age) were purchased from The University of Texas Southwestern Medical Center at Dallas mouse breeding core – the Wakeland Colony. All animal studies were performed in compliance with the research protocol approved by The University of Texas Southwestern Institutional Animal Care and Use Committee. The tumor-bearing animal model was established by injecting a cell suspension (2.5×10^6 cells in 100 μL) subcutaneously into the right and left shoulders of SCID mice. After injection, the general health of the animals was monitored three times a week. The tumor was first visible in the third week and allowed to grow a total of five weeks prior to PET-CT imaging. Tumor volume (mm^3) was calculated using the ellipsoid formula (π/6 × length × width × depth).

RNA isolation and PCR analysis of VEGFR2 expression

Total RNA was extracted from the frozen mouse salivary glands (n = 3) and PC3 tumor tissues (n = 3) using the Rneasy Mini Kit (Qiagen). One microgram of total RNA from each tissue sample was revers transcribed using the iScript Kit

(BioRad). VEGFR2 and GAPDH specific cDNA were amplified using specific primers designed using Primer Express Software (Applied Biosystems). Following cDNA synthesis, an equal amount of cDNA was used for each PCR assay. The PCR was run for 30 cycles by repeating denaturation at 95°C for 1 min, annealing 58 °C for 2 min and polymerization at 72 °C for 1 min using Taq polymerase (Applied Biosystems). The amplicons were run on a 2% agarose gels with ethidium bromide in the running buffer. The intensity of the VEGFR2 and GAPDH amplicons was evaluated by ImageJ Software. The intensity was expressed in arbitrary units. Intensity of the VEGFR2 band was normalized to the GAPDH mean intensity.

Preparation of DOTA-GU40C4 and DOTA-P_{ctrl}

The peptoids were synthesized following a published procedure [10, 13]. To a solution of 2.4 mg (3.05 μmol) maleimido-mono-amide-DOTA (Macrocyclics Inc., Dallas, TX) in 0.25 mL 10 mM phosphate buffer containing 10 mM ethylenediaminetetraacetic acid (EDTA) (pH 7.4) was added 1.4 mg (0.49 μmol) of GU40C4 or 1 mg (0.38 μmol) of the control peptoid (P_{ctrl}). The mixture was then stirred at room temperature for 20 h. The mixture was directly purified by semi-preparative HPLC with gradient (I). The collected fractions from multiple runs were pooled and lyophilized to afford a white solid (yield: ~ 40%). MALDI-TOF/MS: DOTA-GU40C4 ($C_{164}H_{274}N_{40}O_{35}S$): Calculated 3398.2 [m/z], Found: 3420.7 $[M + Na]^+$; DOTA-P_{ctrl} ($C_{144}H_{240}N_{34}O_{43}S$): Calculated 3165.7 [m/z], Found 3166.1 $[M + H]^+$.

Preparation of FITC-GU40C4

To a solution of 3 mg (1.0 μmol) GU40C4 in 0.3 mL 0.1 M phosphate buffer plus 1 mM EDTA (pH 6.9) was added a solution of 0.43 mg (1.0 μmol) N-(5-Fluoresceinyl)maleimide in 20 μL DMSO. The mixture was then stirred in dark at room temperature for 20 h. The mixture was directly purified by semi-preparative HPLC with gradient (II). The collected fractions from multiple runs were pooled and lyophilized to afford a yellow solid (yield: 35%). MALDI-TOF/MS: FITC-GU40C4 ($C_{166}H_{253}N_{35}O_{33}S$), Calculated 3299.1 [m/z]; Found 3299.7 $[M + H]^+$.

VEGFR2 Binding Assay

White, clear bottom 96-well plates (Corning Inc.) were coated with 50 μL of 1 μg/mL recombinant human VEGFR2 protein (R&D Systems) in sensitizing buffer (0.62 g of $NaHCO_3$ and 0.28 g of Na_2CO_3 dissolved on 100 mL of H_2O, pH 9.5) and were kept overnight at 4 °C. The solution was removed and the wells were washed 5 times with 200 μL of the washing buffer (1 × PBS with 0.05% Tween-20, PBS: phosphate buffered saline). The wells were blocked for 30 min with 150 μL of Startingblock blocking buffer (Pierce). After the removal of the blocking buffer, 50 μL of FITC-GU40C4 300 nM in blocking buffer was added to each well. Then, 50 μL of a series of dilutions of GU40C4, DOTA-GU40C4, or DOTA- P_{ctrl} in blocking buffer was added to each well and incubated for 1 h at room temperature (n = 4). After removal of the solution, the wells were washed 5 times with 200 μL of the washing buffer. After addition of 100 μL of 1× PBS

buffer to each well, the remaining fluorescence was measured at 520 nm using a fluorescence plate reader (Synergy HT Multi-Mode Microplate Reader, BioTek®, VT). This competitive binding assay was repeated for three times.

Radiolabeling peptoid conjugates with ^{64}Cu

To a 1.5 mL vial containing 3 μg DOTA-GU40C4 or DOTA-P_{ctrl} in 100 μL of 0.4 M NH_4OAc solution (pH = 6.5), 2 – 3 mCi of ^{64}Cu in 0.1 N HCl was added. The reaction mixture was vortexed and incubated at 37 ºC. After 30 min, 5 μL of 5 mM diethylenetriaminepentaacetic acid (DTPA) was added to the reaction mixture, which was further incubated for 5 min. The reaction mixture was then loaded to a pre-activated light Sep-Pak C-18 cartridge. The ^{64}Cu labeled conjugates were eluted from the cartridge by using 60% ethanol in H_2O. The radiolabeling reaction was monitored by radio-TLC on ITLC-SG plates developed by 1× PBS. The radiochemical purity of the products was determined by radio-HPLC on a Waters Xterra column (150 × 4.6 mm, 5 μm). The mobile phase was H_2O with 0.1% TFA (solvent A) and acetonitrile with 0.1% TFA (solvent B). The gradient consisted of 5% B to 20 % B in 0 – 5 min and 20% B to 40% B in 5–25 min at 1.0 mL/min.

Determination of partition coefficients

Both H_2O-saturated 1-octanol and 1-octanol-saturated H_2O were used for the determination of partition coefficients. Approximately, 0.11 MBq (10 μL) of ^{64}Cu-DOTA-GU40C4 or ^{64}Cu-DOTA-P_{ctrl} was added to a 1.5 mL vial containing 490 μL of 1-octanol-saturated H_2O and 500 μL of H_2O-saturated 1-octanol. The mixture was vigorously vortexed for 1 min at room temperature. After centrifugation at 12,500 rpm for 5 min, a 100 μL aliquot from each layer was measured using a γ-counter (PerkinElmer). The experiment was performed in quintuplicates.

Small animal PET-CT imaging

Small animal PET-CT imaging studies were performed on a Siemens Inveon PET-CT Multimodality System (Siemens Medical Solutions Inc., Knoxville, TN, USA) when the PC3 tumors reached the size of 2 – 6 mm in diameter (n = 3 in each group). A 3.7 MBq dose was injected into the mouse via the tail vein. Ten minutes prior to imaging, the animal was anesthetized using 3% isoflurane at room temperature until stable vitals were established. Once the animal was sedated, the animal was placed onto the imaging bed under 2% isoflurane anesthesia for the duration of the imaging. The microCT imaging was acquired at 80 kV and 500 μA with a focal spot of 58 μm. The total rotation of the gantry was 360° with 360 rotation steps obtained at an exposure time of approximately 235 ms/frame. The images were attained using a CCD readout of 4096 × 3098 with a bin factor of 4 and an average frame of 1. Under low magnification the effective pixel size was 103 μm. Total microCT scan time was approximately 6 min. CT images were reconstructed with a down sample factor of 2 using Cobra Reconstruction Software. The PET imaging was acquired directly following the acquisition of CT data. Static PET scans were performed at 1 h, 4 h, and 20 h post injection (p.i.) for 15 min. PET images were reconstructed using Ordered Subsets Expectation Maximization 3D (OSEM3D) and OSEM2D algorithms.

Reconstructed CT and PET images were fused and analyzed using the Siemens Inveon Research Workplace (IRW) software. The regions of interest (ROIs) were drawn on OSEM2D images for quantitative analysis. The tissues examined include the left and right tumors, the heart, liver, lung, kidney, and muscle. The resulting quantitative data were expressed as percent injected dose per gram of tissue (%ID/g).

Statistical analysis

Statistical analyses were performed using GraphPad Prism. A p value less than 0.05 (unpaired two-tailed t test) was considered statistically significant. All results are presented as mean ± standard deviation.

Results

Preparation of peptoid conjugates

During the combinatorial library screening of peptoids against VEGFR2, the Nleu-Nlys-Nlys (Nleu: *N*-Isobutylglycine; Nlys: N-(4-aminobutyl)glycine) residues at the C-terminus were fixed, while six other residues varied to yield "hits" for optimal VEGFR2 binding. Therefore, the negative control peptoid dimer, P_{ctrl}, consists of six randomly selected peptoid residues at the N-terminus while maintaining the Nleu-Nlys-Nlys trimer at the C-terminus. A lysine-β-alanine-γ-aminohexanoic acid linker was used to construct both GU40C4 and P_{ctrl}. The dimeric peptoids were synthesized according to the published procedure [10, 13]. For ^{64}Cu labeling, DOTA was chosen as the bifunctional chelator to construct the peptoid conjugates. Generally, DOTA conjugation to biomolecules is performed through amide bond formation. However, given the fact that there are multiple amine groups in the peptoids, a C-amide cysteine was introduced as a handle for the DOTA conjugation so that the VEGFR2 binding of GU40C4 was not compromised (**Figure 1**). The DOTA moiety was coupled to the thiol group using a commercially available DOTA-maleimide agent (maleimido-mono-amide-DOTA). To avoid the potential oxidation of the thiol group or unwanted dimerization of the peptoids catalyzed by trace metal ions, all reaction media containing 10 mM EDTA were pre-treated with Chelex® 100 resin. The obtained peptoid conjugates were further purified by semi-preparative HPLC and characterized by MALDI-TOF/MS. The overall yields of the DOTA conjugation were about 40%.

VEGFR2 binding assay

The VEGFR2 binding affinity of the peptoid conjugates was determined by an ELISA-based competitive binding assay. The DOTA-GU40C4 conjugate showed a similar inhibition profile when compared to the intact GU40C4 (GU40C4: IC_{50} = 756 ± 14 nM; DOTA-GU40C4: IC_{50} = 623 ± 98 nM; p = 0.25), while the DOTA-P_{ctrl} conjugate did not display any inhibition effect (**Figure 2**).

Radiolabeling of peptoid conjugates

Both DOTA-GU40C4 and DOTA-P_{ctrl} conjugates were labeled with ^{64}Cu at 37°C in 0.4 M NH_4OAc buffer (pH 6.5) within 30 min in high radiochemical yields (> 90%). The free and nonspecifically bound ^{64}Cu was removed by DTPA at the end of radiolabeling reaction. The reaction mixture was sampled onto an ITLC-SG plate, which was then developed by PBS. Under this TLC condition, both ^{64}Cu labeled peptoid conjugates stayed at the origin, while ^{64}Cu-DTPA moved to the solvent front. The ^{64}Cu-DTPA was removed by passing the reaction mixture through a light C18 Sep-Pak cartridge and washing with H_2O. The product was efficiently eluted with 60% of ethanol in water. The radiochemical purity of ^{64}Cu labeled peptoid conjugates was >98% after the Sep-Pak purification as determined by radio-HPLC. Both ^{64}Cu labeled peptoid conjugates remained intact (> 99%) after being kept in 1× PBS at 37 °C for 24 h.
Both ^{64}Cu-DOTA-GU40C4 and ^{64}Cu-DOTA-P_{ctrl} are slightly hydrophilic, as indicated by their logP values measured in the biphasic mixture of 1-octanol/water (– 0.04 ± 0.01 and – 0.61 ± 0.03, respectively; n = 5).

Small animal PET-CT imaging

The small animal PET-CT imaging evaluation of ^{64}Cu labeled peptoid conjugates was performed in SCID mice bearing PC3 tumors in both left and right shoulders. The representative PET-CT images at 1, 4, and 20 h p.i. (n = 3) are presented in **Figure 3**. The PC3 tumors were clearly visualized by ^{64}Cu-DOTA-GU40C4 at all the three time points. It is important to note that a similar uptake level of the tracer was observed in the left and right tumors. For better clarification, only the image slices cutting through the left tumor are shown (**Figure 3. left**).

The PET images were quantitatively analyzed using the manufacture's software. The quantitative uptake values in the regions of interest (PC3 tumors, heart, liver, lung, kidney, muscle, and salivary glands) are presented in **Table 1**. The tumor accumulation of ^{64}Cu-DOTA-GU40C4 remained steady within 20 h p.i. (2.25 ± 0.24, 2.15 ± 0.34, and 1.90 ± 0.18 %ID/g at 1, 4 and 20 h p.i., respectively) with only an insignificant ~15% drop (p = 0.06). As the activity was gradually cleared from other organs over 20 h, the tumor imaging contrast became enhanced as indicated by the increase of the tumor/muscle ratio (T/N) from 4.73 ± 0.69 at 1 h p.i. to 5.40 ± 0.39 at 4 h p.i. to 6.99 ± 0.92 at 20 h p.i. In contrast, the tumor uptake of ^{64}Cu-DOTA-P_{ctrl} was in the range of 0.3 – 0.5 %ID/g, which was much lower than ^{64}Cu-DOTA-GU40C4 (p < 0.001 at all time points). Interestingly, the salivary glands of the mice were clearly revealed by ^{64}Cu-DOTA-GU40C4 but not by ^{64}Cu-DOTA-P_{ctrl} (**Figure 3** and **Table 1**). The uptake level of ^{64}Cu-DOTA-GU40C4 in the salivary glands was even higher than in the tumors at the early time points (1 h p.i.: 3.17 ± 0.25 %ID/g, p = 0.004; 4 h p.i.: 3.00 ± 0.36 %ID/g, p = 0.02). At 20 h p.i., the uptake in the salivary glands was at the same level as in the tumors (20 h p.i. in the salivary glands: 1.83 ± 0.21 %ID/g, p = 0.65). In contrast, ^{64}Cu-DOTA-P_{ctrl} was found only with close to the background uptake in the salivary glands (0.2 – 0.4 %ID/g at all time points, p < 0.001).

In addition to the significant uptake differences in PC3 tumors and salivary glands, ^{64}Cu-DOTA-GU40C4 and ^{64}Cu-DOTA-P_{ctrl} also differed in their uptake/clearance profiles. Shown in **Figure 3** and **Table 1**, ^{64}Cu-DOTA-P_{ctrl} displayed a much lower background than ^{64}Cu-DOTA-GU40C4. Indeed, the uptake of ^{64}Cu-DOTA-P_{ctrl} was significantly lower in the heart, lungs, and muscle ($p < 0.001$). The highest uptake of ^{64}Cu-DOTA-GU40C4 was observed in the liver (24.03 ± 0.90, 24.40 ± 0.78, and 18.53 ± 1.31 %ID/g at 1, 4 and 20 h p.i., respectively), while that of ^{64}Cu-DOTA-P_{ctrl} *p* was in the kidneys (43.47 ± 4.35, 41.53 ± 3.07, and 30.43 ± 5.66 %ID/g at 1, 4 and 20 h p.i., respectively). These might result from the structure difference of the peptoids.

The specific uptake of ^{64}Cu-DOTA-GU40C4 in salivary glands was supported by the PCR analysis for VEGFR2 mRNA. Salivary glands and PC3 tumors were taken from the same batch of PC3 tumor bearing mice. As observed for the PC3 tumors, the mRNA of VEGFR2 was also clearly present in the salivary glands (**Figure 4A**). However, it is important to note that the band intensity shown in **Figure 4A** is not indicative of the relative mRNA levels of VEGFR2 in the two organs because quantitative PCR was not performed.

Discussion

The goal of this study was to develop a peptoid construct for noninvasive imaging of VEGFR2 expression using the newly reported GU40C4 specific VEGFR2 peptoid. Although peptoids were first introduced in early 1990's, few efforts have been seen to apply this new class of compounds for imaging. Actually, peptoids possess many desired features for *in vivo* imaging applications. For instance, peptoids can form well-defined three dimensional structures in solution to mimic peptides and proteins to specifically bind the corresponding cell surface receptors [14]. Peptoids are highly resistant to enzymatic degradation, which can provide peptoid-based imaging probes with superior *in vivo* stability. Peptoids have demonstrated low immunogenicity, which is a highly desirable *in vivo* property for imaging and therapeutic agents [11]. Large libraries of peptoids in the millions can be synthesized inexpensively and rapidly with precisely defined sequences and chain lengths up to ~ 50 units by modern combinatorial chemistry techniques [14]. This offers abundant opportunities to screen and identify candidates with high specific binding to a biomarker of interest, e.g. VEGFR2. The major obstacle of using peptoids for imaging is their relatively low binding affinities to their specific targets (typically > 1 μM) [15], which is not within the ideal range (0.1–100 nM) for the development of receptor-based imaging probes. Motivated by a report that a library selected peptoid sequence against VEGFR2 can be constructed in a dimeric form (GU40C4) with nanomolar level binding affinity (K_d = 30 nM) [10], this work was set out to develop this unique peptoid construct for PET imaging of VEGFR2, a validated biomarker of angiogenesis.

Given the structural similarities of GU40C4 to conventional peptide constructs, a general peptide modification approach was utilized to construct the peptoid conjugates for labeling with ^{64}Cu by using the most commonly used macrocyclic bifunctional chelator, DOTA. Copper-64 ($t_{1/2}$ = 12.7 h) was chosen because of the unknown *in vivo* kinetics and relatively large size of GU40C4 conjugate and the commercial availability of the PET radioisotope. Given that the

pharmacophore of GU40C includes both side chain and main chain residues [16], we reasoned that any modifications of one or more $-NH_2$ groups in the side chain residues might compromise the VEGFR2 binding affinity. Therefore, a cysteine was positioned at the C-terminus to keep the conjugation site away from the central pharmacophore and enable a site-specific coupling with DOTA via the well established thiol-maleimide chemistry. The DOTA conjugation was straightforward; however the purification of the resulting peptoid conjugates required an iterative HPLC approach due to the insignificant polarity change before and after the DOTA conjugation. The *in vitro* binding assay demonstrated a negligible effect of the DOTA conjugation on the VEGFR2 binding affinity of GU40C4, which warrants the further evaluation of the GU40C4 conjugate. As expected, no specific binding of DOTA-P_{ctrl} was observed to VEGFR2 because it lacks the pharmacophore [16], validating its role as the negative control.

The ^{64}Cu labeling of the peptoid conjugates was highly efficient as indicated by radiochemical yields (>90%). The removal of excess DOTA-peptoid conjugates after radiolabeling, however, was not pursued. Because this would compromise the desired high specific activity of the ^{64}Cu-labeled agents, a series of combinations with decreasing conjugate and increasing ^{64}Cu were tested to attain the highest achievable specific activity. The specific activity reached the 10 – 80 GBq/μmol range. The *in vitro* stability was tested in a PBS buffer and rat serum, while the *in vivo* stability was assessed by analyzing tissue homogenates harvested from mice at 1 h following the injection of the ^{64}Cu-labeled peptoid conjugates. Radio-TLC or radio-HPLC was used in both cases. The method worked well for both conjugates incubated in PBS buffer, which showed 100% intact radiolabeled conjugate within 24 h. However, the stability analyses performed using rat serum and tissue homogenates turned out to be methodically impractical likely due to the highly positive charge of the agents, which led to a strong association with serum proteins. This phenomenon was also reflected by the high liver uptake of the agents in mice as described below. Despite their positively charged nature, both ^{64}Cu-labeled agents only exhibited a modest level of hydrophilicity, which might give arise to a balanced activity clearance through liver and kidney *in vivo*.

The *in vivo* behavior of ^{64}Cu-DOTA-GU40C4 and ^{64}Cu-DOTA-P_{ctrl} was evaluated in SCID mice bearing PC3 prostate cancer xenografts, which were previously shown to highly express VEGFR2 [17]. Because angiogenesis generally occurs when solid tumors reach 2 – 3 mm in diameter [18], the PET-CT imaging experiments were performed with mice bearing tumors in the similar size range. Consistent with the published results our PCR analysis showed a significant level of VEGFR2 mRNA expression in these PC3 tumors. As anticipated, the PC3 tumors were clearly visualized by ^{64}Cu-DOTA-GU40C4 but not with ^{64}Cu-DOTA-P_{ctrl}, the negative control, strongly indicating the VEGFR2 mediated uptake of ^{64}Cu-DOTA-GU40C4. Interestingly, a significant accumulation of ^{64}Cu-DOTA-GU40C4 was also observed in the salivary (submandibular) glands of the mice. This observation is consistent with previous immunohistochemistry studies that have shown intense VEGFR2 expression in the salivary glands [19]. The imaging findings were validated by qualitative PCR analysis which showed that the VEGFR2 mRNA was unequivocally present in the salivary glands of the tumor-bearing mice. The comparative amounts of VEGFR2 mRNA in the salivary glands and tumors cannot be stated since we did not perform quantitative PCR. It is not difficult to envision clinical applications of this observation. For example, in

patients with suspected sialoadenitis or tumors, the VEGR2 expression might change with disease state. Moreover, since it is known that head and neck cancer tumor cells may overexpress VEGFR2, ^{64}Cu-DOTA-GU40C4 may be potentially used for staging the neck or looking for distant spread [20].

Compared to other reported VEGFR2-targeted imaging agents, the tumor uptake level of ^{64}Cu-DOTA-GU40C4 is only modest. For instance, the uptake of ^{64}Cu-DOTA-VEGF$_{121}$ was 3.0 – 4.6 %ID/g in 100 – 200 mm^3 4T1 tumors within 20 h p.i. [8] and 14.9 – 16.3 %ID/g in 4 – 6 mm U87MG tumors within 23 h p.i. [7]; while that of ^{64}Cu-DOTA-VEGF$_{DEE}$ was 3.5 – 5.0 %ID/g in 100 – 200 mm^3 4T1 tumors within 20 h p.i. [8]. Three major factors may account for the tumor uptake differences. First, different tumor models express different levels of VEGFR2, which in turn affects the uptake level of VEGFR2-targeted agents. Second, the VEGFR2 expression level varies with tumor growth, resulting in different uptake levels as the tumor grows even in the same tumor model [7]. Third, in some cases, non-specific tumor uptake could also account for the difference. For instance, the tumor uptake of ^{64}Cu-DOTA-VEGF$_{121}$ in the blockade group only dropped to ~10 %ID/g in U87MG tumors [7], which clearly indicates that ^{64}Cu-DOTA-VEGF$_{121}$ lacks VEGFR2 binding specificity. Although ^{64}Cu-DOTA-GU40C4 showed a relatively low uptake level in PC3 tumors, its steady tumor uptake retention and efficient clearance from non-target organs within the 20 h study period (~2%ID/g) afforded superior tumor imaging contrast, a result that can be attributed to the cell permeable feature of the peptoid conjugate rendered by its positive charge [21] and rapid *in vivo* kinetics resulting from the low molecular weight. This uptake and retention feature might potentiate the utility of peptoid conjugates as theranostic agents.

The major clearance pathways for ^{64}Cu-DOTA-GU40C4 and its control counterpart, ^{64}Cu-DOTA-P$_{ctrl}$ differed greatly due to the charge and hydrophilicity differences of the peptoid conjugates. While ^{64}Cu-DOTA-P$_{ctrl}$ was mainly excreted from the kidneys, ^{64}Cu-DOTA-GU40C4 was cleared by both the renal and hepatic routes. The higher hydrophilicity of ^{64}Cu-DOTA-P$_{ctrl}$ The *in vivo* dislocation of ^{64}Cu from the DOTA moiety might partially cause significant liver uptake [22], which can be tested with other chelators with stronger *in vivo* stability such as the newly reported cross-bridged tetraazamacrocyclic analogs [23]. As implicated in the *in vitro* serum and *in vivo* stability assays, aggregation likely occurred between the highly positively charged GU40C4 conjugate and negatively charged serum proteins or surface proteins of the cells lining the blood vessels inside the liver through electrostatic interactions [24]. The liver deposition of ^{64}Cu-DOTA-GU40C4 could be also enhanced by phagocytosis in the reticuloendothelial system as the consequence of such aggregation [24, 25]. Intriguingly, significantly lower liver uptake was observed for the less positively charged ^{64}Cu-DOTA-P$_{ctrl}$. The unwanted aggregation probably can be alleviated by introduction of polyethylene glycol (PEG) as a linker between GU40C4 and the chelator. While the PEG linker cannot prevent the electrostatic interactions, it may provide steric hindrance to the binding sites in the reticuloendothelial system so as to reduce the liver uptake [24].

Currently, low binding selectivity between VEGFR1 and VEGFR2 is the major drawback of the reported PET probes for VEGFR2 imaging. Due to the expression of VEGFR1, the PET probes inevitably had high accumulation in kidneys or

other non-target organs [7]. Without exception, GU40C4 binds to both VEGFR1 and VEGFR2 with a similar affinity [10]. Therefore, it is desirable to screen new peptoids with higher binding specificity to VEGFR2.

In conclusion, we have shown that ^{64}Cu-DOTA-GU40C4, a dimeric peptoid construct, can be used to noninvasively detect the expression of VEGFR2. Given the role of VEGFR2 in tumor angiogenesis and the versatility of peptoid chemistry, we believe peptoid-based agents will play an increasing role in cancer diagnosis and treatment.

Acknowledgement

This work was partially supported by grants from the National Institutes of Health (P01 DK058398; U24 CA126608; UL1 RR024982), and the Universidad de Guanajuato (000024/10). The authors acknowledge the generous support of a private donor that allowed the purchase of the Inveon PET-CT system.

Disclaimer of Conflict of interest: none.

References

[1] Holmes K, Roberts OL, Thomas AM and Cross MJ. Vascular endothelial growth factor receptor-2: structure, function, intracellular signalling and therapeutic inhibition. Cell Signal 2007; 19: 2003-2012.

[2] Dijkgraaf I and Boerman OC. Molecular imaging of angiogenesis with SPECT. Eur J Nucl Med Mol Imaging 2010; 37 Suppl 1: S104-113.

[3] Guo S, Colbert LS, Fuller M, Zhang Y and Gonzalez-Perez RR. Vascular endothelial growth factor receptor-2 in breast cancer. Biochim Biophys Acta 2010; 1806: 108-121.

[4] Li S, Peck-Radosavljevic M, Kienast O, Preitfellner J, Havlik E, Schima W, Traub-Weidinger T, Graf S, Beheshti M, Schmid M, Angelberger P and Dudczak R. Iodine-123-vascular endothelial growth factor-165 (123I-VEGF165). Biodistribution, safety and radiation dosimetry in patients with pancreatic carcinoma. Q J Nucl Med Mol Imaging 2004; 48: 198-206.

[5] Blankenberg FG, Mandl S, Cao YA, O'Connell-Rodwell C, Contag C, Mari C, Gaynutdinov TI, Vanderheyden JL, Backer MV and Backer JM. Tumor imaging using a standardized radiolabeled adapter protein docked to vascular endothelial growth factor. J Nucl Med 2004; 45: 1373-1380.

[6] Chan C, Sandhu J, Guha A, Scollard DA, Wang J, Chen P, Bai K, Lee L and Reilly RM. A human transferrin-vascular endothelial growth factor (hnTf-VEGF) fusion protein containing an integrated binding site for (111)In for imaging tumor angiogenesis. J Nucl Med 2005; 46: 1745-1752.

[7] Cai W, Chen K, Mohamedali KA, Cao Q, Gambhir SS, Rosenblum MG and Chen X. PET of vascular endothelial growth factor receptor expression. J Nucl Med 2006; 47: 2048-2056.

[8] Wang H, Cai W, Chen K, Li ZB, Kashefi A, He L and Chen X. A new PET tracer specific for vascular endothelial growth factor receptor 2. Eur J Nucl Med Mol Imaging 2007; 34: 2001-2010.

[9] Simon RJ, Kania RS, Zuckermann RN, Huebner VD, Jewell DA, Banville S, Ng S, Wang L, Rosenberg S, Marlowe CK and et al. Peptoids: a modular approach to drug discovery. Proc Natl Acad Sci U S A 1992; 89: 9367-9371.

[10] Udugamasooriya DG, Dineen SP, Brekken RA and Kodadek T. A peptoid "antibody surrogate" that antagonizes VEGF receptor 2 activity. J Am Chem Soc 2008; 130: 5744-5752.

[11] Astle JM, Udugamasooriya DG, Smallshaw JE and Kodadek T. A VEGFR2 antagonist and other peptoids evade immune recognition. Int J Pept Res Ther 2008; 14: 223-227.

[12] Lee J, Udugamasooriya DG, Lim HS and Kodadek T. Potent and selective photo-inactivation of proteins with peptoid-ruthenium conjugates. Nat Chem Biol 2010; 6: 258-260.

[13] De León-Rodríguez LM, Lubag A, Udugamasooriya DG, Proneth B, Brekken RA, Sun X, Kodadek T and Dean Sherry A. MRI Detection of VEGFR2 in Vivo Using a Low Molecular Weight Peptoid–(Gd)8 -Dendron for Targeting. J Am Chem Soc 2010; 132: 12829-12831.

[14] Seo J, Barron AE and Zuckermann RN. Novel peptoid building blocks: synthesis of functionalized aromatic helix-inducing submonomers. Org Lett 2010; 12: 492-495.

[15] Fowler SA and Blackwell HE. Structure-function relationships in peptoids: recent advances toward deciphering the structural requirements for biological function. Org Biomol Chem 2009; 7: 1508-1524.

[16] Udugamasooriya DG, Dunham G, Ritchie C, Brekken RA and Kodadek T. The pharmacophore of a peptoid VEGF receptor 2 antagonist includes both side chain and main chain residues. Bioorg Med Chem Lett 2008; 18: 5892-5894.

[17] Stadler WM, Cao D, Vogelzang NJ, Ryan CW, Hoving K, Wright R, Karrison T and Vokes EE. A randomized Phase II trial of the antiangiogenic agent SU5416 in hormone-refractory prostate cancer. Clin Cancer Res 2004; 10: 3365-3370.

[18] Folkman J. Tumor angiogenesis: therapeutic implications. N Engl J Med 1971; 285: 1182-1186.

[19] Swelam W, Ida-Yonemochi H, Maruyama S, Ohshiro K, Cheng J and Saku T. Vascular endothelial growth factor in salivary pleomorphic adenomas: one of the reasons for their poorly vascularized stroma. Virchows Arch 2005; 446: 653-662.

[20] Neuchrist C, Erovic BM, Handisurya A, Steiner GE, Rockwell P, Gedlicka C and Burian M. Vascular endothelial growth factor receptor 2 (VEGFR2) expression in squamous cell carcinomas of the head and neck. Laryngoscope 2001; 111: 1834-1841.

[21] Kwon YU and Kodadek T. Quantitative evaluation of the relative cell permeability of peptoids and peptides. J Am Chem Soc 2007; 129: 1508-1509.

[22] Boswell CA, Sun XK, Niu WJ, Weisman GR, Wong EH, Rheingold AL and Anderson CJ. Comparative in vivo stability of copper-64-labeled cross-bridged and conventional tetraazamacrocyclic complexes. J Med Chem 2004; 47: 1465-1474.

[23] Liu W, Hao GY, Long MA, Anthony T, Hsieh JT and Sun XK. Imparting Multivalency to a Bifunctional Chelator: A Scaffold Design for Targeted PET Imaging Probes. Angew Chem Int Edit 2009; 48: 7346-7349.

[24] Liu F and Liu D. Serum independent liposome uptake by mouse liver. Biochim Biophys Acta 1996; 1278: 5-11.

[25] Willmann JK, Cheng Z, Davis C, Lutz AM, Schipper ML, Nielsen CH and Gambhir SS. Targeted microbubbles for imaging tumor angiogenesis: assessment of whole-body biodistribution with dynamic micro-PET in mice. Radiology 2008; 249: 212-219.

Table 1. Uptake of ^{64}Cu-DOTA-GU40C4 and ^{64}Cu-DOTA-P_{ctrl} in major organs of interest determined by quantitative PET imaging analysis. Data are presented as %ID/g ± standard deviation (n = 3). * $p = 0.06$; † $p = 0.004$; ‡ $p = 0.02$; § $p = 0.65$.

	^{64}Cu-DOTA-GU40C4			^{64}Cu-DOTA-P_{ctrl}		
	1 h	4 h	20 h	1 h	4 h	20 h
Tumor	*†2.25 ± 0.24	‡2.15 ± 0.34	*§1.90 ± 0.18	0.34 ± 0.12	0.30 ± 0.14	0.51 ± 0.19
Salivary glands	†3.17 ± 0.25	‡3.00 ± 0.36	§1.83 ± 0.21	0.28 ± 0.08	0.22 ± 0.04	0.42 ± 0.10
Heart	1.30 ± 0.27	1.50 ± 0.20	1.30 ± 0.26	0.31 ± 0.11	0.32 ± 0.05	0.65 ± 0.04
Lung	2.03 ± 0.32	1.77 ± 0.31	1.33 ± 0.06	0.32 ± 0.11	0.42 ± 0.13	0.52 ± 0.01
Liver	24.03 ± 0.90	24.40 ± 0.78	18.53 ± 1.31	13.57 ± 1.38	12.27 ± 1.67	11.63 ± 1.56
Kidney	6.57 ± 1.34	6.50 ± 1.23	5.07 ± 0.91	43.47 ± 4.35	41.53 ± 3.07	30.43 ± 5.66
Muscle	0.49 ± 0.07	0.37 ± 0.06	0.26 ± 0.02	0.14 ± 0.03	0.12 ± 0.04	0.12 ± 0.03

Figure legends:

Figure 1. Structures of the DOTA peptoid conjugates: (A) DOTA-GU40C4, (B) DOTA-P_{ctrl}

Figure 2. Self competitive binding isotherms of GU40C4 against VEGFR2 derived from ELISA-like experiments. Concentration gradients of GU40C4, DOTA-GU40C4, and DOTA-P_{ctrl} competed with a fixed amount (300 nM) of FITC-GU40C4 on VEGFR2 coated ELISA plates. GU40C4: IC_{50} = 756±14 nM; DOTA-GU40C4: IC_{50} = 623±98 nM; p =0.25, R^2 > 0.9. No inhibition effect was shown by DOTA-P_{ctrl} on the FITC-GU40C4 binding.

Figure 3. Representative PET-CT images of ^{64}Cu-DOTA-GU40C4 and ^{64}Cu-DOTA-P_{ctrl} in PC3 tumor-bearing mice at 1, 4, and 20 h p.i. For simplicity, one-side tumors are focused for presentation because the left/right tumors were not in the same plane**.** Tumors are indicated by yellow arrows; salivary glands are indicated by red arrows.

Figure 4. (A) Agarose gel electrophoresis of PCR products showing specificity of RT-PCR for VEGFR2. Lane M, 1 kb DNA size marker; lanes 1 – 3, salivary glands; lanes 4 – 6, PC3 tumor; lanes 7, non-template control. (B) Sequences of primers for PCR. An amplicon of the expected 200 bp was clearly generated from cDNA preparations of salivary glands and PC3 tumor xenografts.

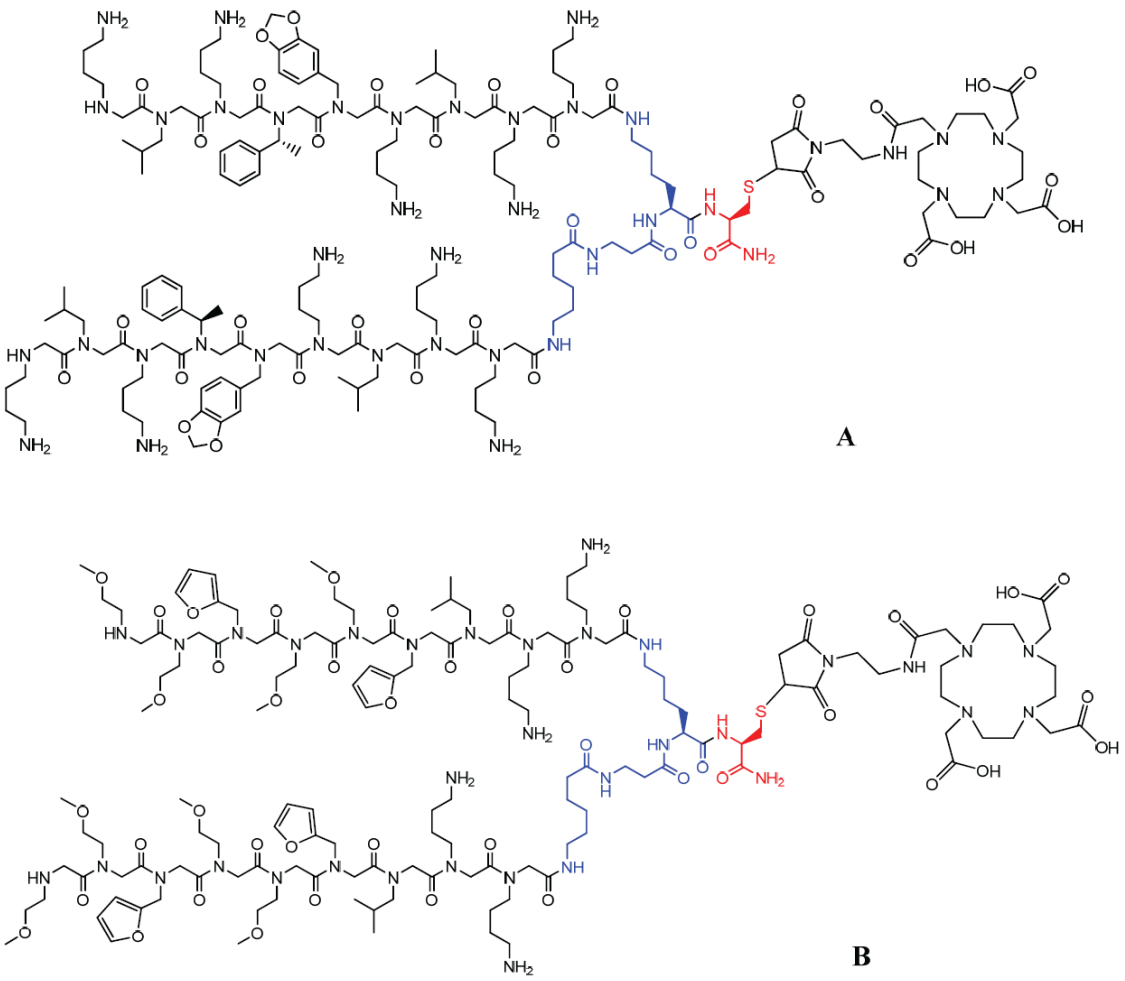

Figure 1

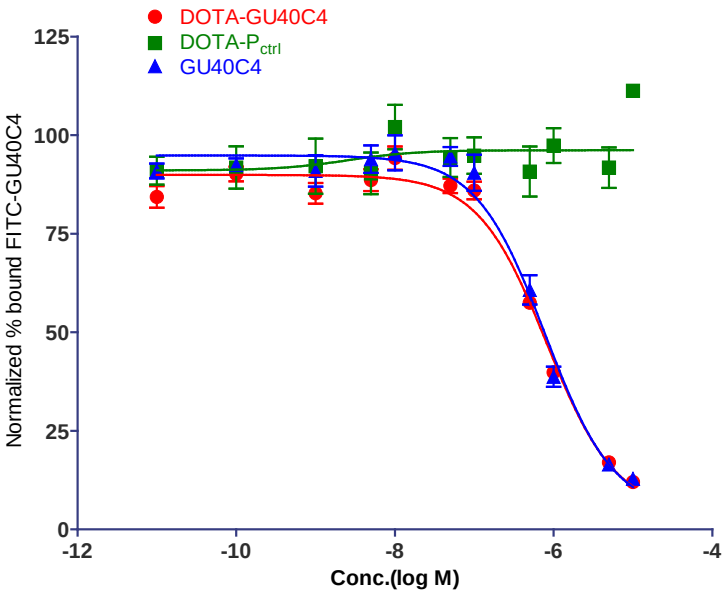
DOTA-GU40C4
DOTA-P$_{ctrl}$
GU40C4
Normalized % bound FITC-GU40C4
125
100
75
50
25
0
-12
-10
-8
-6
-4
Conc.(log M)

Figure 2

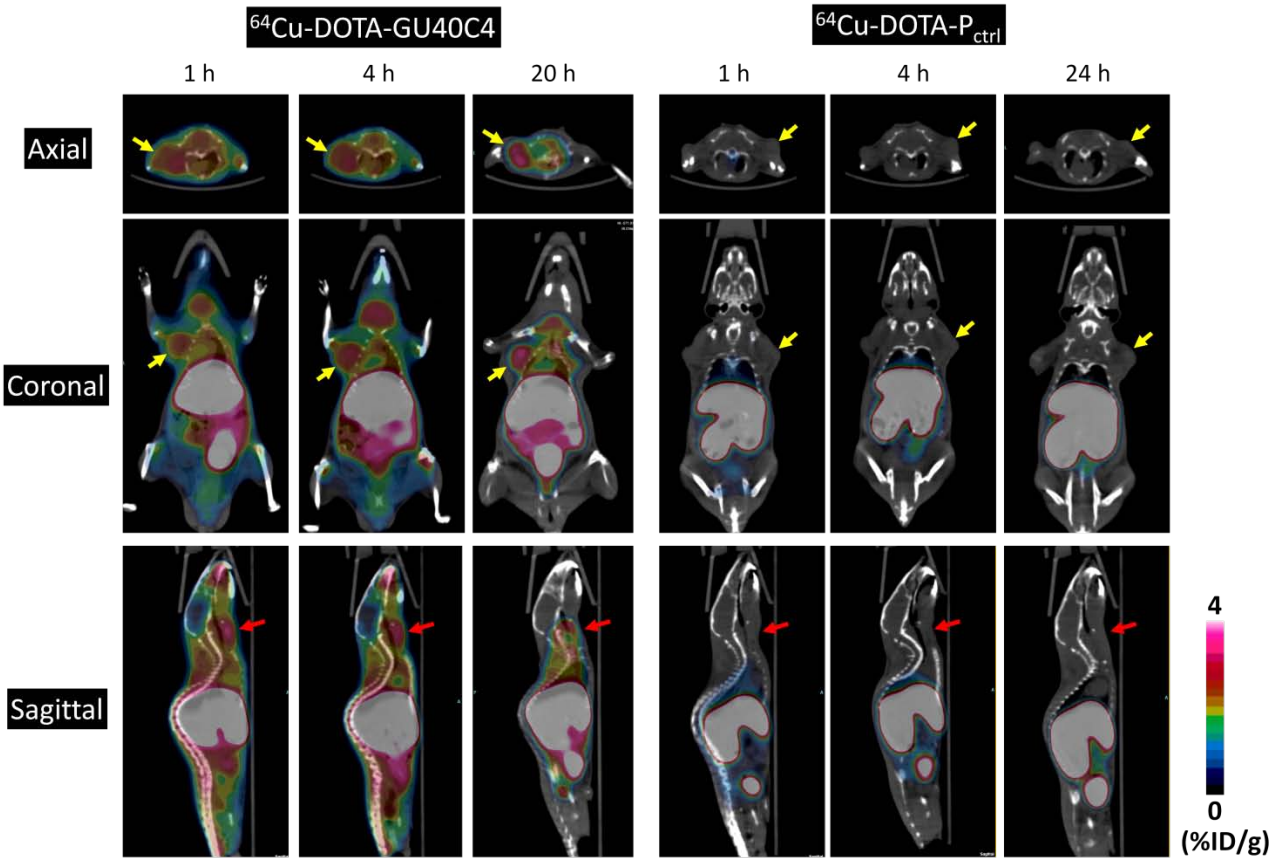
64Cu-DOTA-GU40C4
64Cu-DOTA-Pctrl
1 h
4 h
20 h
1 h
4 h
24 h
Axial
Coronal
Sagittal
4
0
(%ID/g)

Figure 3

A.

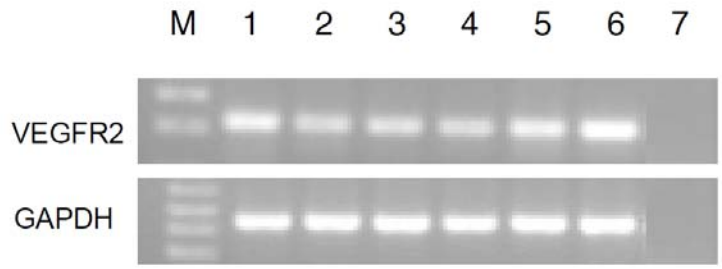

B.

	VEGFR2	Mouse GAPDH
Forward primer	GCAAAACACTCACCATTCCCA	CTGCCATTTGCAGTGGCAAAGTGG
Reverse primer	GAGGTTTGAAATCGACCCTCG	TTGTCATGGATGACCTTGGCCAGG

Figure 4